Materials Advances

ROYAL SOCIETY OF CHEMISTRY

PAPER

View Article Online
View Journal | View Issue

Cite this: *Mater. Adv.*, 2024, 5, 2545

Investigating the effect of CeO_2 on the radical scavenging activity of Pt@CoO_x/NC@CeO_2 during the electrocatalytic oxygen reduction reaction in acidic and alkaline environments†

Fatima Nasim,[a] Hassan Ali,[a] Amir Waseem [a] and Muhammad Arif Nadeem *[ab]

Researchers have concentrated on developing electrocatalysts that are especially designed to minimise oxygenated radicals generated in partial oxygen reduction reactions (ORRs). Herein, we report Pt@CoO_x/NC@$CeO_2$1 as a cost-effective, stable, and highly durable electrocatalyst in both 0.1 M KOH and 0.1 M $HClO_4$ electrocatalytic environments with low platinum loading (*ca.* 5% only). Outstanding results are delivered by the Pt@CoO_x/NC@$CeO_2$1 with half-wave potential ($E_{1/2}$) ~ 0.89 V_{RHE} in 0.1 M KOH. The optimized electrocatalyst, *i.e.*, Pt@CoO_x/NC@$CeO_2$1, is also found to be efficient for the ORR in 0.1 M $HClO_4$ with $E_{1/2}$ ~ 0.89 V_{RHE} compared to 20 wt% Pt/C. The innovative support (CoO_x/NC) obtained through facile calcination of ZIF-12 has been deposited over porous ceria nanorods (CeO_2). The platinum nanoparticles are then decorated over CoO_x/NC@CeO_2. To investigate the influence of cobalt on the electrocatalytic ORR process, platinum-decorated commercial multiwalled carbon nanotubes (Pt@MWCNTs1) were synthesized using the same synthetic methodology. The as-synthesized electrocatalyst (Pt@CoO_x/NC@$CeO_2$1) demonstrates enhanced mass activity (MA) of ~263 mA mg_{Pt}^{-1} in 0.1 M KOH and 231 mA mg_{Pt}^{-1} in 0.1 M $HClO_4$ at their $E_{1/2}$ and an enhanced electrochemical active surface area (ECSA) of ~261 m^2 g^{-1}. The material also demonstrates radical scavenging activity resulting in enhanced durability with a significant amount of current retention for 30 h in both alkaline (99.8%) and acidic electrolytes (99.9%).

Received 14th January 2024,
Accepted 30th January 2024

DOI: 10.1039/d4ma00041b

rsc.li/materials-advances

Introduction

The development of sustainable and green energy technology to meet the ever-increasing demands of the growing world is a hot topic under immense debate. Among the various technologies, proton exchange membrane fuel cells (PEMFCs) have drawn substantial consideration during the past several years due to their renewable, clean and efficient nature.[1] PEMCs offer high conversion efficiency and low operating temperature, but still their widespread application is limited by the slow chemical steps of the ORR and deteriorating performance over time due to chemical, mechanical and electrochemical degradation of cell components, *i.e.*, the polymeric membrane, support, and catalyst.[2–4] The ORR generally proceeds *via* four electron and two electron reduction pathways.[5] The reactive oxygen species (ROS) including singlet oxygen ($^{\bullet}O$), hydroxyl radicals ($^{\bullet}OH$), and hydroperoxide radicals ($^{\bullet}OOH$) are derived from molecular oxygen during the insufficient ORR process.[4,6] These species containing unpaired electrons are highly reactive and significantly hamper the durability of the PEMFCs by the degradation of the membrane over time and poisoning of the catalyst. Generally, platinum deposited carbon has been reported as an effective catalyst to increase the sluggish kinetics of the ORR.[7] However, the aggregation of platinum nanoparticles leading to reduction in the preliminary ECSA and degradation of the carbon support during the operating conditions of PEMFCs is yet a challenge that has to be resolved.[8] Alloying Pt NPs with other transition metals and chemical doping are the most widely used methods to enhance the catalytic activity and efficiency of the synthesized catalysts. However, despite the extensive research in this field, the stability of platinum-transition metal-based alloys remains a great challenge due to the speedy discharge of transition metals in the acidic environment of PEMFCs.[4] Nadeem and co-workers synthesized Pt-Ni/PC 950 with enhanced catalytic activity, minimizing the usage of Pt. However, the catalyst retained only 25% of the initial current density in the acidic environment after 500 cycles.[9] Several reports suggest that metal oxides as additives or an

[a] *Department of Chemistry, Quaid-i-Azam University, Islamabad 45320, Pakistan*
[b] *Pakistan Academy of Sciences, 3-Constitution Avenue Sector G-5/2, Islamabad, Pakistan. E-mail: manadeem@qau.edu.pk*

† Electronic supplementary information (ESI) available. See DOI: https://doi.org/10.1039/d4ma00041b

alternative support can enhance the catalytic activity of the cathode material for the ORR as well as provide mechanical strength, corrosion resistance and high stability under harsh operating conditions of PEMFCs.[10–12] The strong interaction of the loaded metal and support material, also called strong metal support interaction (SMSI), modulates the electronic properties of the material, which has a direct influence on the Fermi level of the material.[10] The surface energy of the loaded nanoparticles is reduced, which leads to increased electrocatalytic activity.[13] The electric potential of the materials containing carbon effectively overcomes the challenges linked with the use of transition metal oxides such as sintering, dissolution, agglomeration and poor electrochemical properties.[14,15] Recently, transition metal nanoparticles stabilized by quantum dots have been shown to be an electrochemically active catalyst for the evolution reaction of hydrogen (HER) by Weifeng *et al.*[16] Similarly, an electrocatalyst (α-Fe_2O_3/GO) synthesized by Xiangqian *et al.* has shown superior ORR activity than α-FeOOH, and α/γ-FeOOH supported over graphene oxide (GO).[17] Dena *et al.* have shown that mixed transition metal oxides (MTMOs) supported over activated carbon (MnO_2-CuO/AC, and CoO-CuO/AC) more efficiently catalyse the ORR compared to the same metal oxides supported over graphene.[18] Among several transition metal oxides, ceria (CeO_2) has been proven to be an effective candidate for enhancing the overall performance of PEMFCs. The varying oxidation states of CeO_2 enable it to transition between Ce^{3+} and Ce^{4+}, facilitating its involvement in scavenging ROS generated during suboptimal ORR electrocatalysis. This characteristic of CeO_2 alleviates the deterioration rate of the proton exchange membrane (PEM) by capturing radicals such as $^{\bullet}OH$, $^{\bullet}O$, $^{\bullet}OOH$, and $^{\bullet}H$.[19–22] For example, Ki Ro *et al.* reported interfacial doping of CeO_2 into a Pt/C electrocatalyst for increasing the overall functioning of the PEMFC.[4] Similarly D'Urso *et al.* synthesized a silica-supported cerium-oxide-based radical scavenger bearing sulfonic acid functionalities. The synthesized material improved the life time of PEMFCs.[21] Recent research suggests that carbon nanomaterials such as MWCNTs, graphene, functionalized quantum dots and fullerenes could participate in scavenging activity and removing the ROS from the fuel cells by forming adducts, hydrogen donation and electron transfer.[6,23–25] Lifeng *et al.* reported chlorine doped quantum dots exhibiting scavenging activity towards ROS.[6] Similarly Ana *et al.* reported the scavenging activity of CNTs and found that zigzag CNTs are better electron donors and acceptors.[25] Besides scavenging activity, MWCNTs also provide high surface area and excellent mechanical and electrical properties and can be used as an alternative carbonaceous support.[26,27] The unique one-dimensional shape of CNTs allows for excellent ionic transport resulting in fascinating activity in the electrochemical field.[28] In view of the above considerations, modifying the outer surface of cobalt oxide incorporated nitrogen-doped tubular carbon (NC) with CeO_2 having Pt NP deposition on the surface can be a good choice for scavenging ROS along with the increased catalytic activity and efficiency towards the ORR. The scavenging ability of NC and CeO_2 enhances the durability of the catalyst and in turn improves the lifetime of PEMFCs.

Experimental

Synthesis of ceria nanorods (CeO_2)

4 mmol of cerium nitrate hexahydrate ($Ce(NO_3)_3{\cdot}6H_2O$) and 0.5 mmol of sodium hydroxide (NaOH) were dissolved in 30 ml of distilled water and stirred for 30 minutes. The resulting blend was moved to an autoclave. The temperature of the autoclave was then gradually raised to 140 °C and maintained at that temperature for 14 h. The synthesized material was cooled to ambient temperature and separated through filtration. The obtained product was washed with distilled water to eliminate impurities and then dried out in an oven at 60 °C. Subsequently, the dried sample underwent annealing at 400 °C for 1 h to yield CeO_2 nanorods.

Synthesis of ZIF-12@CeO_2

400 mg of CeO_2 was disseminated in 20 mL distilled water for 1 h. 1.318 mmol of cobalt nitrate hexahydrate ($Co(NO_3)_2$. $6H_2O$) and 6.09 mmol of benzimidazole ($C_7H_6N_2$) were liquefied in 20 mL *N*,*N*-dimethylformamide (DMF) and added to the dispersed CeO_2. An autoclave with Teflon lining was used to heat the prepared mixture at 150 °C in an oven for two days. The autoclave was then allowed to cool to ambient temperature, yielding the crystalline product. The obtained product was washed many times with distilled water and DMF to eliminate any contaminants or unreacted components. Upon drying, the material was ready for subsequent procedures.

Synthesis of CoO_x/NC@CeO_2 (calcination of ZIF-12@CeO_2)

The synthesised material (ZIF-12@CeO_2) was calcined using heating equipment. The reaction occurred at elevated temperatures in an inert atmosphere. 200 mg of ZIF-12@CeO_2 was heated to 850 °C for 8 h in a tube furnace. After cooling to room environment, the product was used as a support material in the manufacture of ORR electrocatalysts.

Synthesis of catalysts (Pt@CoO_x/NC@CeO_2)

The catalyst was obtained by the polyol reduction method. 20 mg of chloroplatinic acid ($H_2PtCl_6{\cdot}H_2O$) was dissolved and stirred in 10 mL ethylene glycol at 70 °C for 30 min. After that, 70 mg of CoO_x/NC@CeO_2 dispersed in 20 mL ethylene glycol was added dropwise. The temperature of the mixture was gradually raised to 180 °C and refluxed for 4 h until the formation of Pt nanoparticles. Upon the completion of the reaction, the whole system was permitted to cool down. Afterwards, the material was collected and rinsed many times with distilled water and methanol to eliminate any contamination. Different materials having various amounts of precursor metal salt ($H_2PtCl_6{\cdot}H_2O$) were synthesised by employing the same methodology. The electrocatalytic activities of these materials towards the ORR were determined to find out the effect of the

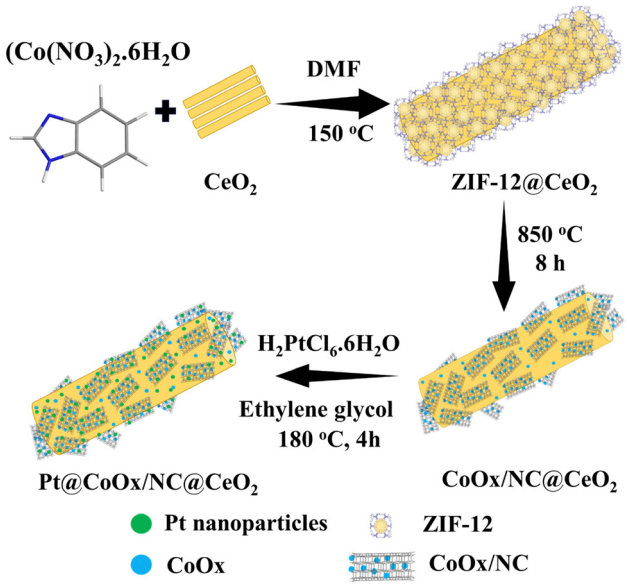

Scheme 1 Synthetic procedure of Pt@CoO_x/NC@CeO_2s.

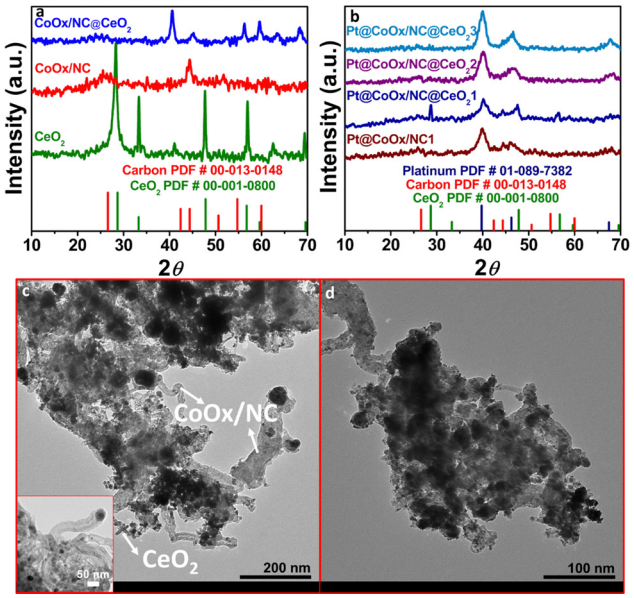

Fig. 1 (a) X-ray diffraction pattern of CeO_2, CoO_x/NC and CoO_x/NC@CeO_2. (b) X-ray diffraction pattern of Pt@CoO_x/NC1 and Pt@CoO_x/NC@CeO_2s. (c) TEM analysis of Pt@CoO_x/NC@$CeO_2$1 at 200 nm. (d) TEM analysis of Pt@CoO_x/NC@$CeO_2$1 at 100 nm.

concentration of platinum metal. 20 wt% Pt/C was synthesized for comparison by the polyol reduction method using Vulcan XC-72. The synthetic methodology for the fabrication of Pt@CoO_x/NC@CeO_2s is given in Scheme 1.

Electrochemical investigations

To electrocatalytic ability of the materials was estimated using a three-electrode system. A rotating disc electrode (RDE) with a carbon disc functioned as the working electrode, while Hg/HgO and a graphite rod were employed as reference and counter electrodes, respectively. The working electrode was manufactured by drop-casting 2.5 μL of the synthesized ink carefully on the RDE to fabricate the working electrode, which was obtained by the sonication of 2 mg of the catalyst in a combination of 100 μL isopropanol and 5% Nafion. The linear sweep voltammetry (LSV) technique was utilized to assess the materials' capacity to reduce oxygen in both 0.1 M $HClO_4$ and 0.1 M KOH in an O_2-saturated atmosphere, at 10 mV s^{-1}. The current provided was normalised by the RDE's area (0.19625 cm^2). The ECSA was determined using the Pt–O layer reduction method, where a complete monolayer of Pt–O was formed at 1.4 V_{RHE} through cyclic voltammetry (CV) at 50 mV s^{-1} in 0.1 M $HClO_4$. Catalyst stability was assessed through an accelerated durability test (ADT) conducted over 10 000 CV cycles, while long-term durability was determined *via* chronoamperometric measurements over a 30 h period. All experiments were conducted at room temperature with a catalyst loading of 2.5 μL. The scavenging potential was evaluated by measuring its absorption using a UV-visible spectrophotometer. Antioxidant activity was determined by employing a $DPPH^{\bullet}$-ethanol solution (2 mg/25 mL ethanol).

Results and discussion

The powder X-ray diffraction (PXRD) of the synthesized materials was used to determine the purity of the sample. The PXRD of all the synthesized materials has been shown in Fig. 1a and b. Figure a shows the X-ray diffraction analysis of CeO_2, CoO_x/NC and CoO_x/NC@CeO_2. The diffraction peaks of CeO_2 match well with the standard reference card of CeO_2 (JCPDS card no. 00-001-0800), which confirms the successful formation of ceria nanorods. The peaks at 25.8° and 44.37° in the diffractogram of (CoO_x/NC) correspond to the (002) and (101) plane of graphitic carbon (JCPDS card no. 00-013-0148). The peaks for cobalt oxides (CoO_x) are not noticeable in the diffraction patterns due to the very low quantity of cobalt. The diffraction peaks of CeO_2 at $2\theta \sim 28.4°$, 33.28°, and 47.6° are not visible in the PXRD result of CoO_x/NC@CeO_2 owing to overlap of CeO_2 by CoO_x/NC. The PXRD analysis of all the materials revealed that a graphitic carbon network has been retained throughout the synthetic procedure (Fig. 1b). The PXRD of Pt@CoO_x/NC1 shows the formation of platinum nanoparticles by the emergence of peaks at 39.98°, 46° and 68° (JCPDS card no. 01-089-7382). In Pt@CoO_x/NC@$CeO_2$1, the peaks at 28.80°, 47.7° and 56.56° correspond to the (111), (220) and (311) planes of CeO_2. The remaining peaks correspond to graphitic carbon and platinum nanoparticles. In Pt@CoO_x/NC@$CeO_2$2 and Pt@CoO_x/NC@$CeO_2$3, the peaks corresponding to CeO_2 are not visible due to the greater concentration of platinum nanoparticles, which covers the surface of the CeO_2 (Fig. 1b). The PXRD patterns of all the synthesized materials match well with their corresponding reference patterns, indicating the phase purity and homogeneity of the samples. Fig. S1 (ESI†) shows the PXRD pattern of the MWCNTs and Pt@MWCNTs1.

Scanning transmission electron microscopy (SEM) and transmission electron microscopy (TEM) were used to determine the morphology of Pt@CoO_x/NC@$CeO_2$1. SEM findings noticeably depict the presence of CeO_2 masked by CoO_x/NC

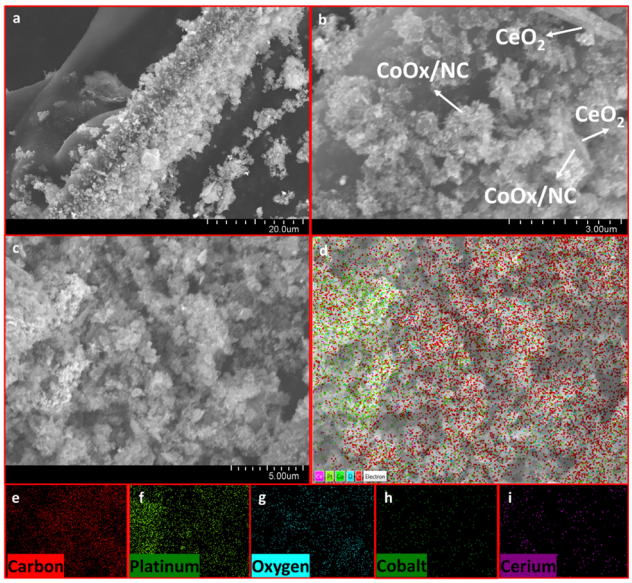

Fig. 2 SEM analysis of Pt@CoO_x/NC@$CeO_2$1: (a) 20 μm, (b) 3 μm and (c) 5 μm; (d) elemental mapping of Pt@CoO_x/NC@$CeO_2$1: (e) carbon, (f) platinum, (g) oxygen, (h) cobalt and (i) cerium.

(Fig. 2a and b). Elemental mapping further validates the occurrence of cerium, cobalt, platinum, oxygen, carbon, and nitrogen (Fig. 2e–i). SEM analysis reveals a significant overlap between CeO_2 and CoO_x/NC, contributing to the intensified activity towards the ORR. The detectible portion of CeO_2 contributes to the scavenging potential of the material, expected to intercept ROS produced during incomplete ORR, thereby improving the material's endurance in challenging electrocatalytic environments.

TEM analysis of Pt@CoO_x/NC@$CeO_2$1 supports the findings of SEM. The appearance of tubular carbon can be clearly seen in the TEM analysis (Fig. 1c and d). The ends of the tubular carbon are encapsulated by CoO_x nanoparticles. Ceria nanorods can also be present but as the CoO_x/NC surrounds the CeO_2 (supported by SEM analysis) they are seldom found in the TEM analysis of Pt@CoO_x/NC@$CeO_2$1. The interconnected nodes in tubular carbon provide anchoring sites for the successful deposition of platinum nanoparticles. The porous nature of CeO_2 supports the adsorption of oxygenated radicles, thus inhibiting the deterioration of the catalyst during the inadequate ORR. Fig. S2 (ESI†) shows the HRTEM exploration of CoO_x/NC at a resolution of 10 nm.

To find the surface elemental composition of Pt@CoO_x/NC@$CeO_2$1, X-ray photoelectron spectroscopy (XPS) analysis was performed (Fig. 3). The XPS clearly indicates the presence of all constituents in the optimized electrocatalyst (Pt@CoO_x/NC@$CeO_2$1). The deconvolution of the 2p core level of cobalt specifies the presence of metallic cobalt species at a binding energy (B.E) value ~779.5 eV corresponding to the $2p_{3/2}$ region. The peak at B.E value ~781.6 eV confirms the formation of Co^{2+} species in the Pt@CoO_x/NC@$CeO_2$1. The fitted region of Co $2p_{1/2}$ also reveals the peaks at B.E value ~796.7 eV. The peaks at 786.1 eV and 802.6 eV represent the shaking fragments of the Co 2p region (Fig. 3a). The XPS spectrum of platinum gives

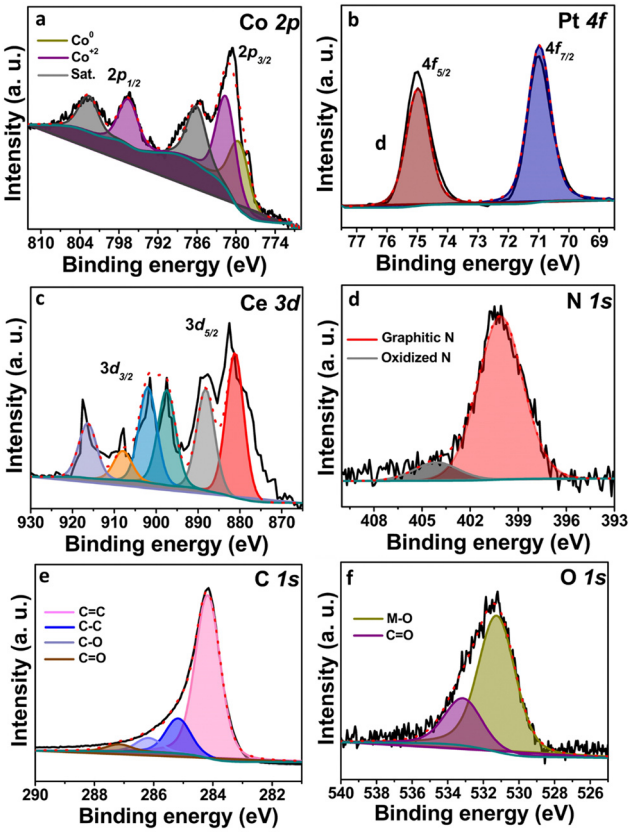

Fig. 3 XPS of Pt@CoO_x/NC@$CeO_2$1: (a) Co 2p, (b) Pt 4f, (c) Ce 3d, (d) N 1s, (e) C 1s and (f) O 1s.

two peaks in the fitted region at 70.9 eV and 74.9 eV corresponding to Pt $4f_{7/2}$ and Pt $4f_{5/2}$, respectively (Fig. 3b). These values suggest that platinum exists purely in metallic form (standard B.E of Pt nanoparticles ~71.0 eV) as no peaks for platinum oxide have been observed in the fitted envelop of Pt 4f. Fig. 3c reveals the multiplet spectrum of Ce 3d. The deconvoluted Ce 3d core level consists of six peaks giving three peaks in each spin orbit state (Ce $3d_{5/2}$ and Ce $3d_{3/2}$). The peaks at B.E values ~400 eV and 404.1 eV correspond to graphitic nitrogen and oxidized nitrogen, respectively, in the nitrogen 1s core level (Fig. 3d). The fitted envelop of the C 1s core level has four peaks at 284.1 eV, 285.2 eV, 286.1 eV and 287.2 eV, which correspond to C═C (sp^2 carbon) and C–C (sp^3 carbon) and carbon bonded to oxygen (Fig. 3e). The XPS spectrum of oxygen shows the bonding of oxygen to metals, *i.e.*, cerium and cobalt. The peaks at B.E of 533.1 eV are due to the surface oxygen bonded to the carbon network (Fig. 3f).

The XPS analysis of CoO_x/NC has been shown in Fig. S4 (ESI†). The percentage of platinum metal determined from the atomic absorption spectroscopy (AAS) is 5.3%, 7.1% and 9.2% for Pt@CoO_x/NC@$CeO_2$1, Pt@CoO_x/NC@$CeO_2$2, and Pt@CoO_x/NC@$CeO_2$3, respectively. The EDX analysis of Pt@CoO_x/NC@$CeO_2$1 has been shown in Fig. S3 (ESI†).

Electrochemical investigations

Cyclic voltammetry and linear sweep voltammetry techniques were used to evaluate the ORR electrocatalytic activity of the

synthesized materials in O_2 and Ar saturated 0.1 M KOH and 0.1 M $HClO_4$. The SMSI of the platinum nanoparticles, CeO_2 and support material (CoO_x/NC) greatly enhanced the catalytic activity of the synthesized material. Among all the synthesized materials, the material with minimal amount of Pt (Pt@CoO_x/NC@$CeO_2$1) revealed surprisingly efficient activity compared to the electrocatalysts having greater concentration of platinum. The percentages of cobalt and platinum determined from AAS and XPS were found to be 2.2% and 5.3%, respectively, in Pt@CoO_x/NC@$CeO_2$1. The investigation of the mechanism of ORR on catalysts based on transition metal oxides is still ongoing and requires further exploration. The ideal concentration of cobalt and platinum in Pt@CoO_x/NC@$CeO_2$1 results in increased ORR activity due to the electronic interaction of cobalt and platinum. The increased concentration of platinum has a negative influence on the ORR electrocatalytic activity of Pt@CoO_x/NC@$CeO_2$2 and Pt@CoO_x/NC@$CeO_2$1. From this it can be inferred that the optimum ratio of platinum and cobalt at which the material exhibits the highest electrocatalytic activity is 2 : 5. The binding energies of the oxygenated intermediates produced during the reaction were modulated by the re-distribution of charge densities *via* SMSI, which results in significant variation in the electronic environment around the metal cores, thus facilitating the ORR kinetics.[29,30] All the electrochemical outcomes were related to the reference and benchmark catalysts (Pt/C) under the same environment to govern the effectiveness of the catalysts.

The ORR is a slow reaction which generally proceeds *via* two pathways. The four-electron process (direct pathway) is generally favoured over the two electron process (indirect pathway) due to low overpotential of the reaction steps involved. The effectiveness of the electrocatalysts is determined from the binding strength of the reaction intermediates and the electrocatalyst's surface; a major contributing factor in the efficiency of the catalyst.[31,32] Numerous researchers have reported the significant electrocatalytic role of the Pt-based bimetallic components.[33,34] However, the synthesis of Pt@CoO_x@$CeO_2$1 in this work is noteworthy because of the negligible amount of platinum, which overcomes the cost problem accompanied with the use of noble-metals. RDE was employed to record the ORR activity by performing LSV at various rotations in both acidic and alkaline environments. Fig. 4 and 5 reflect the ORR activity of the as synthesized electrocatalysts in 0.1 M KOH and 0.1 M $HClO_4$ respectively. Fig. 4(b) and 5(b) compare the LSV curves of Pt@CoO_x/NC1 with CeO_2, CoO_x and Pt@CoO_x/NC1 in basic and acidic media, respectively. In terms of MA, the Pt@CoO_x/NC@$CeO_2$1 demonstrated superior ORR catalytic activity among all the presented electrocatalysts in both basic and acidic media, which is higher than 20 wt% Pt/C (Fig. 6b and c respectively). The ECSA of Pt@CoO_x/NC@$CeO_2$1 was found to be 261 $m^2\ g^{-1}$, which is high among all the presented catalysts (Fig. 6e). The reduction of oxide coverage on the surface of the fabricated materials enhanced the ORR activity. To investigate the effect of cobalt in the synthesized materials, platinum nanoparticles were also observed on MWCNTs for comparison (Fig. 4a and 5a).

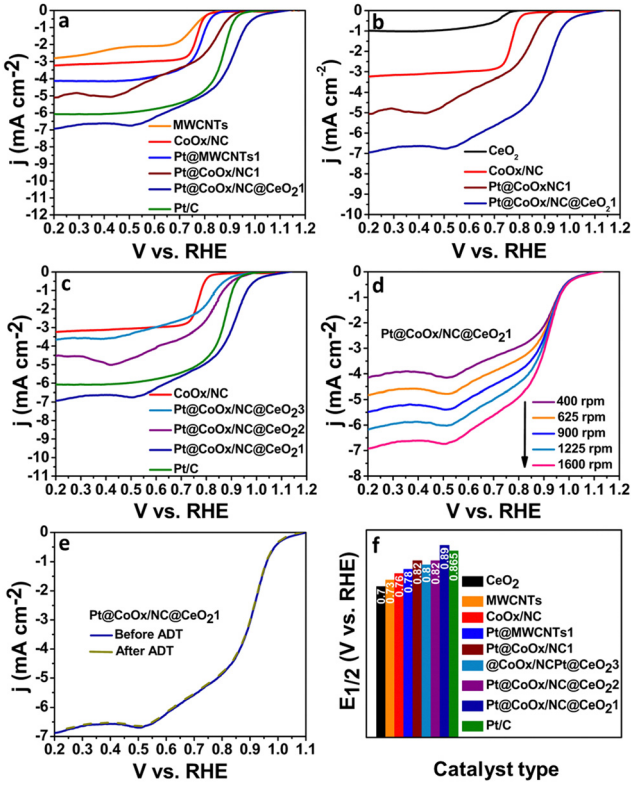

Fig. 4 Electrochemical behaviour of the synthesized materials in 0.1 M KOH at 10 mV s^{-1}: (a) influence of CoO_x on the ORR activity of Pt@CoO_x/NC@$CeO_2$1, (b) comparison of the ORR performance of the optimized electrocatalyst with CeO_2, CoO_x/NC and Pt@CoO_x/NC1, (c) concentration effect of Pt@CoO_x/NC@CeO_2s, (d) influence of rotation on the electrocatalytic ORR performance of Pt@CoO_x/NC@$CeO_2$1, (e) durability test of Pt@CoO_x/NC@$CeO_2$1 over 10 000 cycles and (f) comparison of $E_{1/2}$ of the fabricated materials.

Among all the synthesized materials, Pt@CoO_x/NC@$CeO_2$1 exhibited the highest electrochemical activity towards the ORR in both alkaline and acidic environments. The electrocatalyst demonstrated an onset potential (E_{onset}) of 1.11 V_{RHE}, which is very close to the thermodynamic potential (1.23 V_{RHE}) in 0.1 M KOH (Fig. 4 and Fig. S5b, ESI†). The material also exhibited outstanding $E_{1/2} \sim 0.89\ V_{RHE}$ and a current density of 6.96 mA cm^{-2} in 0.1 M KOH, which is superior to Pt/C (0.86 V_{RHE}, 6.08 mA cm^{-2}), a benchmark and reference catalyst (Fig. 4f and Fig. S5c, ESI†). The accelerated durability test (ADT) and chronoamperometry were executed to explore the durability of the catalysts. The material exhibited no loss in $E_{1/2}$ after 10 000 cycles demonstrating the high stability of the synthesized material (Fig. 4e). Fig. S7 (ESI†) reflects the extended stability of the material over a period of 30 h. The pre- and post-XPS of Pt@CoO_x/NC@$CeO_2$1 in Fig. S9 (ESI†) further confirms the stability of the material. The material Pt@CoO_x/NC@$CeO_2$1 retained 99.8% and 99.9% of its initial current in 0.1 M KOH and 0.1 M $HClO_4$, respectively, after a period of 30 h demonstrating the high stability of the material in harsh electrocatalytic environments on comparison to Pt@CoO_x/NC1, which retained 95% of its initial current in basic environment and

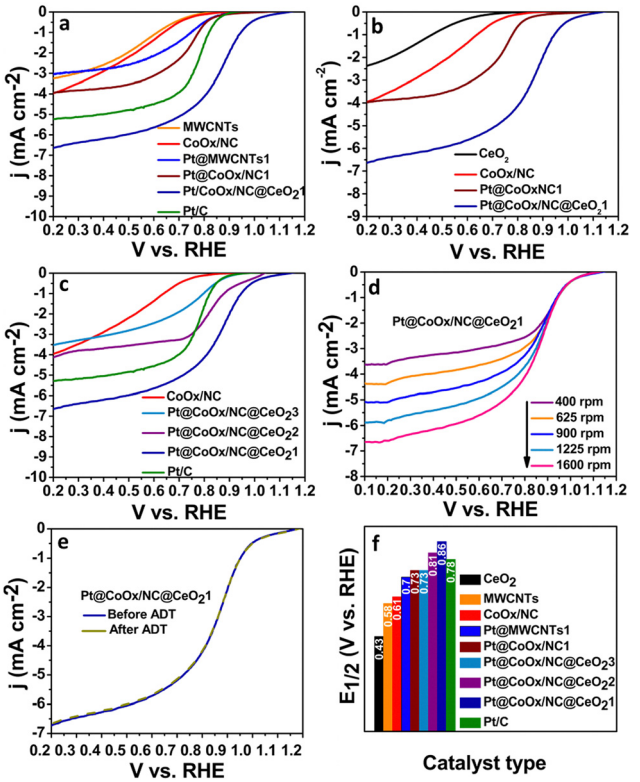

Fig. 5 Electrochemical behaviour of the synthesized materials in 0.1 M $HClO_4$ at 10 mV s^{-1}: (a) effect of CoO_x on the ORR activity of Pt@CoO_x/NC@$CeO_2$1, (b) comparison of the ORR performance of the optimized electrocatalyst with CeO_2, CoO_x/NC and Pt@CoO_x/NC1, (c) concentration effect of Pt@CoO_x/NC@CeO_2s, (d) influence of rotation on the electrocatalytic ORR performance of Pt@CoO_x/NC@$CeO_2$1, (e) durability test of Pt@CoO_x/NC@$CeO_2$1 over 10 000 cycles and (f) comparison of $E_{1/2}$ of the fabricated materials.

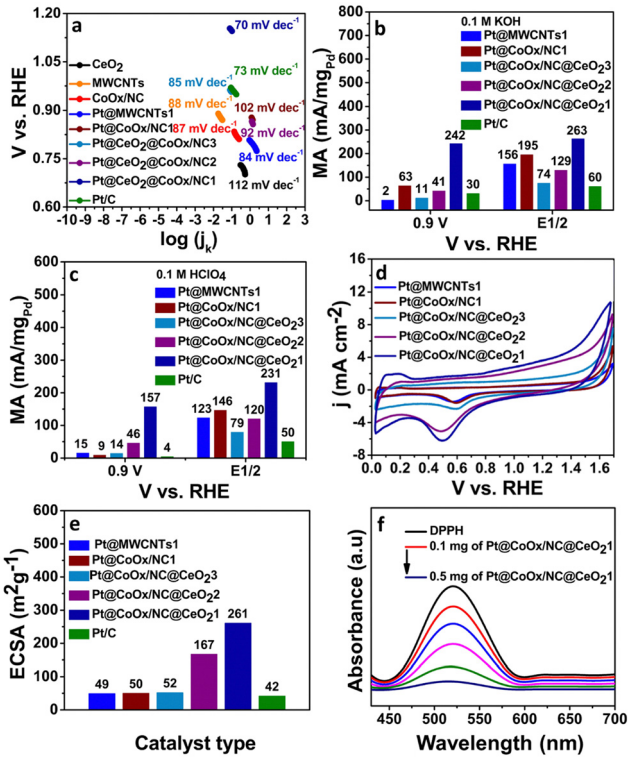

Fig. 6 (a) Tafel slopes of all the materials in 0.1 M KOH, (b) MA of the synthesized electrocatalysts in 0.1 M KOH, (c) MA of the synthesized electrocatalysts in 0.1 M $HClO_4$, (d) CV curves of the Pt-decorated electrocatalysts at the upper potential limit of 1.4 V_{RHE} at 50 mV s^{-1} in an Ar saturated environment, (e) bar graph representing comparison of ECSA of the synthesized electrocatalysts and (f) decrease in the absorption of DPPH$^{\bullet}$-ethanol solution encompassing various amounts of Pt@CoO_x/NC@$CeO_2$1.

76% in acidic media (Fig. S7a and b, ESI†). The high durability of the material is attributed to the decrease in coverage of intermediates formed during the reaction on the surface of platinum, which poison the catalysts. In strongly acidic conditions, the hydrogen ions can react with platinum to form soluble platinum ions. The increased acidity of the solution can enhance the leaching process. Generally, platinum supported on carbon experiences this problem. It has been reported in various literature studies that the incorporation of transition metal oxide in carbon increases the stability of the carbon materials and solves the corrosion problem in harsh electrocatalytic environments. The B.E of Co is shifted from 779.0 eV in CoO_x/NC to 779.5 eV, which is an indication of the electronic interaction of cobalt and platinum. The interaction of platinum with the cobalt and the proper encapsulation of platinum nanoparticles within the support material, *i.e.*, CoO_x/NC@CeO_2, prevents the leaching of platinum in harsh acidic conditions employed during the electrochemical ORR, which has been depicted in the enhanced durability revealed by chronoamperometric measurements over 30 h.

Platinum is renowned as the most efficient metal for catalysing the ORR. However, its prohibitively high cost, coupled with issues related to the adsorption and challenging desorption of oxygenated intermediates, often leads to catalyst poisoning, rendering Pt/C impractical for widespread commercialization. The inclusion of CeO_2 in Pt@CoO_x/NC@CeO_2, as opposed to Pt/C, serves the crucial role of efficiently scavenging harmful radicals, thereby enhancing the stability of our material. CeO_2 is well-known for its porous structure and its ability to scavenge radicals. The presence of CeO_2 effectively transforms the catalyst into an antioxidant, adept at scavenging DPPH radicals, which further contributes to its scavenging capability, ultimately resulting in the material's exceptional durability.

The scavenging activity of the CeO_2 nanostructures is responsible for the enhanced durability of the material in corrosive environments, which engulf the ROS produced during partial ORR, leading to the poisoning of the catalyst. As a control, platinum nanoparticles were also deposited over MWCNTs. The material (Pt@MWCNTs1) demonstrated $E_{1/2}$ of 0.78 V_{RHE}, which is inferior to the $E_{1/2}$ of Pt@CoO_xNC1 in 0.1 M KOH (0.82 V_{RHE}), confirming the role of cobalt in the ORR electrocatalysis (Fig. 4a and f).

To find whether the reaction proceeds *via* a four-electron or two-electron route, the electron transfer number (n) was

calculated. Koutecky–Levich (K–L) plots were drawn by plotting $1/j$ *vs.* $\omega^{1/2}$. From the slope, the value of n was found to be 3.9 in 0.1 M KOH, which is very near to 4, implying the preferable four electron reduction pathway (Fig. S5a, ESI†). The value of n was found to vary with potential and hence the average number of n was calculated in the potential region studied. The kinetics of the reaction were determined by measuring the Tafel slopes. Among all the synthesized materials, Pt@CoO_x/NC@$CeO_2$1 exhibited the lowest Tafel slope $\sim$70 mV dec^{-1}, which is inferior to Pt/C (73 mV dec^{-1}), exhibiting fast reaction kinetics on the surface of Pt@CoO_x/NC@$CeO_2$1 (Fig. 6a).

The ability of the material to reduce oxygen molecules was also investigated in 0.1 M $HClO_4$. Similar to the alkaline environment, the Pt@CoO_x/NC@$CeO_2$1 also delivered outstanding electrocatalytic activity in acidic electrolyte (Fig. 5). The E_{onset} and $E_{1/2}$ of Pt@CoO_x/NC@$CeO_2$1 are superior among all the synthesized electrocatalysts (Fig. S6b and Fig. 5f, respectively, ESI†). Fig. 5 represents the comparison of the LSV curves of all the fabricated materials in 0.1 M $HClO_4$. The electron transfer n was calculated to be 4.2, which suggests four electron pathways (Fig. S6a, ESI†). The MA of Pt@CoO_x/NC@$CeO_2$1 is also very high in acidic environments. Fig. 6b and c represent the comparison of MA of all synthesized electrocatalysts in 0.1 M KOH and 0.1 M $HClO_4$, respectively. The ECSA determines the ability of the material to catalyse the electrochemical reaction. Materials having a larger surface area demonstrate better electrocatalytic activity. The ECSA of all the materials was determined from the Pt–O layer reduction method by recording CV curves in 0.1 M $HClO_4$ (Fig. 6d). The ECSA of all the synthesized materials is in the following order.

Pt@MWCNTs1 < Pt@CoO_x/NC1 < Pt@CoO_x/NC@$CeO_2$3 < Pt@CoO_x/NC@$CeO_2$2 < Pt@CoO_x/NC@$CeO_2$1.

The high ECSA of Pt@CoO_x/NC@$CeO_2$1 is attributed to the uniform dispersion of platinum nanoparticles (Fig. 6e). The interconnected nodes of tubular carbon provide appropriate adsorption positions for the dispersion of platinum nanoparticles leading to facile electrochemical reaction. Fig. S7c (ESI†) represents the CV curve for the determination of ECSA of Pt/C.

It is important to mention that the shape of the ORR polarization is typically square shaped or S shaped. This curve is often associated with the four-electron reduction pathway, where oxygen is reduced to water *via* a sequence of four electron-transfer steps. However, in some cases, the polarization curve may deviate from this typical square shape, and several factors can contribute to this behaviour: the competing two electron pathway leads to variation in the ORR polarization curve. The kinetics of the ORR on the surface of Pt@CoO_x/Nc@CeO_2 are indeed diffusion controlled with no decomposition of the reaction sample occurring during the ORR process. This can be confirmed from the post-XPS analysis, post-SEM, and post-TEM analysis after 30 h of chronoamperometric measurements (Fig. S9–S11 respectively, ESI†). The difference in the ORR polarization curve in 0.1 M KOH and 0.1 M $HClO_4$ is due to the formation of different reaction intermediates in both media, which leads to a different ORR curve. Moreover, changes in electrolyte conditions can influence the kinetics of the ORR. Understanding the specific conditions and factors influencing the ORR in a particular system is essential for interpreting the shape of the polarization curve.

The antioxidant ability of the material was assessed by employing DPPH$^\bullet$ as a representative radical (Fig. 6f). The electrocatalyst formed a bond with DPPH$^\bullet$, which was dispersed in a DPPH$^\bullet$/ethanol solution followed by incubation in the absence of light. UV-visible spectrophotometry was employed to determine the radical scavenging activity of Pt@CoO_x/NC@$CeO_2$1. The DPPH radical exhibited a prominent absorption peak at 518 nm within the 400–700 nm range when no scavenging material was present. Upon the addition of the Pt@CoO_x/NC@$CeO_2$1, a substantial reduction in the absorbance of the DPPH$^\bullet$ occurred, indicating effective scavenging by Pt@CoO_x/NC@$CeO_2$1. The results showed that an increased amount of Pt@CoO_x/NC@$CeO_2$1 led to a notable reduction in the absorbance of DPPH$^\bullet$. Fig. S8 (ESI†) illustrates the residual ratio of DPPH radical following incubation with different concentrations of Pt@CoO_x/NC@$CeO_2$1. The radical scavenging ability of Pt@CoO_x/NC@$CeO_2$1 facilitates strong adsorption of ROS generated in partial ORR catalysis onto the porous structure of CeO_2. This prevents catalyst poisoning and significantly enhances material durability in challenging electrocatalytic environments. The comparison of the synthesized materials in terms of durability with recently reported Pt-based electrocatalysts has been shown in Table 1. Our synthesized material is cost-effective and highly durable compared to the reported literature and commercial 20 wt% Pt/C, which costs approximately half (56%) of the proton exchange membrane fuel cell

Table 1 Comparison of the durability of recent Pt-based electrocatalysts with the present work

Catalyst	Durability ($E_{1/2}$)	Electrolyte	Ref.
Pt@CoO_x@CeO_2/NC1	Does not change (10 000 cycles)	0.1 M KOH	This work
Pt@CoO_x@CeO_2/NC1	Does not change (10 000 cycles)	0.1 M $HClO_4$	This work
$Pt_{83}Ni_{17}$ BNCs AG/C	6.1 mV (20 000 cycles)	0.1 M $HClO_4$	46
Pt/W-doped TiO_2	89 mV (10 000 cycles)	0.1 M $HClO_4$	47
PtFe@Gr/CB	10 mV (10 000 cycles)	0.1 M $HClO_4$	48
Pt/Z438	Changes slightly (10 000 cycles)	0.1 M $HClO_4$	49
MP-PtPb NWs	700 mV (10 000 cycles)	0.1 M $HClO_4$	50
$Pt_{0.23}Cu_{0.64}Co_{0.13}$/C	400 mV (5000 cycles)	0.1 M KOH	51
$Pt_{15}Y_5Al_{80}$	Changes slightly (10 000 cycles)	0.1 M $HClO_4$	52
Pt@C/C700	Changes slightly (10 000 cycles)	0.1 M $HClO_4$	53

stacks.[35] The overall cost of our synthesized catalysts is low compared to Pt/C because of the very low loading of Pt and Ce. Moreover, the commercial Pt/C experiences leaching problems in acidic conditions, which leads to the corrosion and ineffective performance of Pt/C. The commercial Pt/C needs replacement with time, posing hurdles to its commercialization. Our synthesized material is highly durable in both acidic and basic conditions with a retention of nearly 100% current over 30 h of chronoamperometric measurement, which makes it a cost-effective and efficient catalyst to be employed in fuel cell technology.

Role of CeO_2 during the ORR on the surface of Pt@CoO_x@$CeO_2$1

The primary function of CeO_2 in the context of this study is to remove ROS formed in partial reduction of oxygen. This scavenging capability was assessed using UV-visible spectroscopy with DPPH as a model radical. The addition of varying concentrations of the optimized catalyst led to a decrease in DPPH absorbance, confirming the material's scavenging ability. Additionally, the literature extensively supports the co-catalytic role of CeO_2. Its inclusion prevents the formation of the harmful species H_2O_2, which can degrade both the catalyst performance and the proton exchange membrane in fuel cells over time. CeO_2 facilitates the conversion of H_2O_2 to water, mitigating its formation during the ORR, a crucial side reaction in fuel cells.

Additionally, beyond serving as a co-catalyst, CeO_2 offers appropriate sites for the adsorption of oxygen molecules and intermediates produced during the ORR. The envisioned mechanism for ORR on the Pt@CoO_x/NC@CeO_2 surface entails a bidentate mode of adsorption. Although the intricate details of the ORR mechanism on catalysts based on transition metals are still being explored, current research indicates that metal sites supported on nitrogen-doped carbon likely act as active sites.[36,37] The electronic surroundings of Pt are tailored by its interaction with cobalt, optimizing the binding strength for adsorbed oxygenated intermediates and enhancing the ORR activity.[37–39] The interaction of cobalt with platinum alters the electronic surroundings of Pt, optimizing the binding strength for adsorbed oxygenated intermediates and augmenting the activity of the ORR.[40–42]

The variance in electronegativity between platinum and cobalt, coupled with charge redistribution, plays a role in enhancing the activity and durability of the ORR. The enriched electrons from Pt species safeguard carbon nanotubes against erosion and oxidation, thereby improving the stability of Pt@CoO_x/NC@CeO_2.[42,43] The adsorption of O_2 on the surface of Pt nanoparticles stretches the O═O bond, facilitating the easy separation of the O_2 molecule, ultimately leading to the production of ORR products.[44]

The chemisorbed O_2 undergoes protonation to generate *OOH, followed by the separation of the O–OH bond to produce water molecules (see Fig. 7). This implies that CeO_2 offers appropriate adsorption positions for the chemisorption of O_2 and oxygenated intermediates, facilitating the transfer of charge between Ce^{3+} and Ce^{4+} species. This highlights the efficient performance of Pt@CoO_x/NC@CeO_2 in the ORR.

Furthermore, the co-catalytic behaviour of CeO_2 has been extensively explained in the literature.[45] CeO_2 confines toxic radicals generated during the partial reduction of O_2 (production of H_2O_2) and transforms them into water, thereby dropping the possibility of catalyst poisoning. The breakdown of H_2O_2 produces the potent hydroxyl free radical ($^{\bullet}OH$), which, if left unchecked, can attack the proton exchange membrane (PEM) and consequently diminish the material's resilience.[45] The proven scavenging capability of CeO_2 demonstrated through UV-visible spectroscopy addresses this concern. Therefore, incorporating CeO_2 emerges as an effective strategy to enhance the resilience of PEMFCs. The co-catalytic behaviour of CeO_2 is illustrated in the provided equations.

$$O_2 + 2H^+ + 2e^- \rightarrow H_2O_2 \quad (1)$$

$$2CeO_2 + 2H^+ + 2e^- \rightarrow Ce_2O_3 + H_2O \quad (2)$$

$$Ce_2O_3 + H_2O_2 \rightarrow 2CeO_2 + H_2O \quad (3)$$

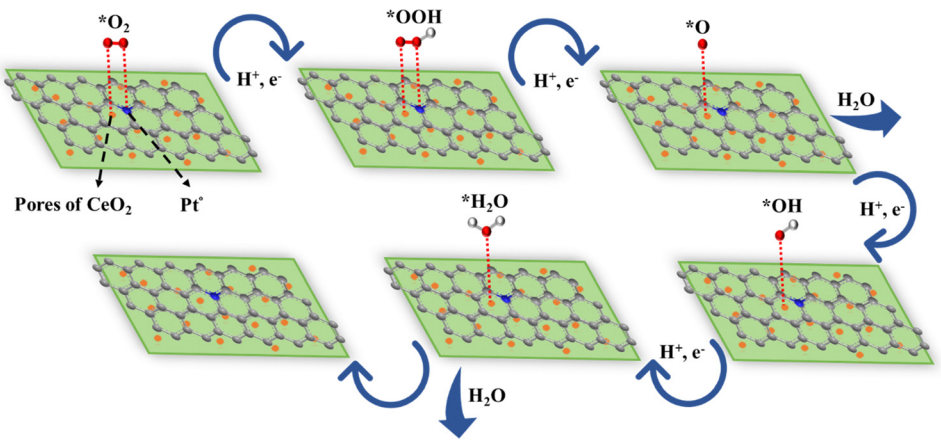

Fig. 7 Mechanism of ORR on the surface of Pt@CoO_x/NC@$CeO_2$1.

Conclusions

A series of economical, applicable, and durable Pt-based electrocatalysts (Pt@CoO_x/NC@$CeO_2$1, Pt@CoO_x/NC@$CeO_2$2, and Pt@CoO_x/NC@$CeO_2$3) with striking ORR behaviour were successfully synthesized *via* the polyol reduction method. All the synthesized electrocatalysts have been investigated for ORR electrocatalytic activity in both alkaline and acidic environments. The optimized electrocatalysts (Pt@CoO_x/NC@$CeO_2$1) exhibited superior activity in terms of $E_{1/2}$ in both alkaline (0.89 V_{RHE}) and acidic environments (0.86 V_{RHE}) with a minimal amount of platinum loading. The as-synthesized electrocatalyst (Pt@CoO_x/NC@$CeO_2$1) also demonstrated increased MA in both 0.1 M KOH and acidic 0.1 M $HClO_4$. The high ORR electrocatalytic activity of Pt@CoO_x/NC@$CeO_2$1 is attributed to its larger ECSA (261 m^2 g^{-1}). The Pt@CoO_x/NC@$CeO_2$1 material actively engages in radical scavenging during the ORR electrocatalytic process, leading to improved durability with a retention of 99.8% and 99.9% current in both alkaline and acidic environments, respectively, over an extended period. The radical scavenging capability of Pt@CoO_x/NC@$CeO_2$1 is endorsed to the porous nature of CeO_2, capturing ROS produced in the partial ORR process, thereby enhancing the catalyst's durability. This study introduces a straightforward, cost-effective, and environmentally friendly method for synthesizing highly efficient electrocatalysts with antioxidant activity, resulting in increased durability in challenging electrocatalytic environments.

Conflicts of interest

There are no conflicts to declare.

Acknowledgements

The work was financially supported by the Pakistan Academy of Sciences (PAS) and Higher Education Commission (HEC) of Pakistan (No. 8400/Federal/NRPU/R&D/HEC/2017).

References

1 S. Chen, Y. Yan, P. Hao, M. Li, J. Liang, J. Guo, Y. Zhang, S. Chen, W. Ding and X. Guo, Iron nanoparticles encapsulated in S,N-codoped carbon: sulfur doping enriches surface electron density and enhances electrocatalytic activity toward oxygen reduction, *ACS Appl. Mater. Interfaces*, 2020, **12**(11), 12686–12695.

2 J. Wu, X. Z. Yuan, J. J. Martin, H. Wang, J. Zhang, J. Shen, S. Wu and W. Merida, A review of PEM fuel cell durability: degradation mechanisms and mitigation strategies, *J. Power Sources*, 2008, **184**(1), 104–119.

3 R. Borup, J. Meyers, B. Pivovar, Y. S. Kim, R. Mukundan, N. Garland, D. Myers, M. Wilson, F. Garzon, D. Wood, P. Zelenay, K. More, K. Stroh, T. Zawodzinski, J. Boncella, J. E. McGrath, M. Inaba, K. Miyatake, M. Hori, K. Ota, Z. Ogumi, S. Miyata, A. Nishikata, Z. Siroma, Y. Uchimoto, K. Yasuda, K.-I. Kimijima and N. Iwashita, Scientific Aspects of Polymer Electrolyte Fuel Cell Durability and Degradation, *Chem. Rev.*, 2007, **107**(10), 3904–3951.

4 K. R. Yoon, J. M. Kim, K. A. Lee, C.-K. Hwang, S. G. Akpe, Y. J. Lee, J. P. Singh, K. H. Chae, S. S. Jang and H. C. Ham, Activity-stability benefits of Pt/C fuel cell electrocatalysts prepared via remote CeO_2 interfacial doping, *J. Power Sources*, 2021, **496**, 229798.

5 S. K. Singh, K. Takeyasu and J. Nakamura, Active sites and mechanism of oxygen reduction reaction electrocatalysis on nitrogen-doped carbon materials, *Adv. Mater.*, 2019, **31**(13), 1804297.

6 L. Wang, Y. Li, Y. Wang, W. Kong, Q. Lu, X. Liu, D. Zhang and L. Qu, Chlorine-doped graphene quantum dots with enhanced anti-and pro-oxidant properties, *ACS Appl. Mater. Interfaces*, 2019, **11**(24), 21822–21829.

7 X. Wang, M. Vara, M. Luo, H. Huang, A. Ruditskiy, J. Park, S. Bao, J. Liu, J. Howe and M. Chi, Pd@ Pt core–shell concave decahedra: a class of catalysts for the oxygen reduction reaction with enhanced activity and durability, *J. Am. Chem. Soc.*, 2015, **137**(47), 15036–15042.

8 J. Choi, J. Cho, C.-W. Roh, B.-S. Kim, M. S. Choi, H. Jeong, H. C. Ham and H. Lee, Au-doped PtCo/C catalyst preventing Co leaching for proton exchange membrane fuel cells, *Appl. Catal., B*, 2019, **247**, 142–149.

9 I. A. Khan, Y. Qian, A. Badshah, M. A. Nadeem and D. Zhao, Highly porous carbon derived from MOF-5 as a support of ORR electrocatalysts for fuel cells, *ACS Appl. Mater. Interfaces*, 2016, **8**(27), 17268–17275.

10 J. Li, H. Zhou, H. Zhuo, Z. Wei, G. Zhuang, X. Zhong, S. Deng, X. Li and J. Wang, Oxygen vacancies on TiO_2 promoted the activity and stability of supported Pd nanoparticles for the oxygen reduction reaction, *J. Mater. Chem. A*, 2018, **6**(5), 2264–2272.

11 A. Lewera, L. Timperman, A. Roguska and N. Alonso-Vante, Metal–Support Interactions between Nanosized Pt and Metal Oxides (WO_3 and TiO_2) Studied Using X-ray Photoelectron Spectroscopy, *J. Phys. Chem. C*, 2011, **115**(41), 20153–20159.

12 M. L. Hernández-Pichardo, R. G. González-Huerta, P. del Angel, M. Tufiño-Velazquez and L. Lartundo, The role of the WO_3 nanostructures in the oxygen reduction reaction and PEM fuel cell performance on WO_3–Pt/C electrocatalysts, *Int. J. Hydrogen Energy*, 2015, **40**(48), 17371–17379.

13 J. Zhang, J. Ma, T. S. Choksi, D. Zhou, S. Han, Y.-F. Liao, H. B. Yang, D. Liu, Z. Zeng, W. Liu, X. Sun, T. Zhang and B. Liu, Strong Metal–Support Interaction Boosts Activity, Selectivity, and Stability in Electrosynthesis of H_2O_2, *J. Am. Chem. Soc.*, 2022, **144**(5), 2255–2263.

14 M. Sun, H. Liu, Y. Liu, J. Qu and J. Li, Graphene-based transition metal oxide nanocomposites for the oxygen reduction reaction, *Nanoscale*, 2015, **7**(4), 1250–1269.

15 C. Goswami, K. K. Hazarika and P. Bharali, Transition metal oxide nanocatalysts for oxygen reduction reaction, *Mater. Sci. Technol.*, 2018, **1**(2), 117–128.

16 W. Chen, J. Shen, Y. Huang, X. Liu and D. Astruc, Catalyzed hydrolysis of tetrahydroxydiboron by graphene quantum dot-stabilized transition-metal nanoparticles for hydrogen evolution, *ACS Sustainable Chem. Eng.*, 2020, **8**(19), 7513–7522.
17 X. Liu and W. Hu, Iron oxide/oxyhydroxide decorated graphene oxides for oxygen reduction reaction catalysis: a comparison study, *RSC Adv.*, 2016, **6**(35), 29848–29854.
18 D. Z. Khater, R. Amin, M. Mahmoud and K. El-Khatib, Evaluation of mixed transition metal (Co, Mn, and Cu) oxide electrocatalysts anchored on different carbon supports for robust oxygen reduction reaction in neutral media, *RSC Adv.*, 2022, **12**(4), 2207–2218.
19 N. J. Lawrence, J. R. Brewer, L. Wang, T.-S. Wu, J. Wells-Kingsbury, M. M. Ihrig, G. Wang, Y.-L. Soo, W.-N. Mei and C. L. Cheung, Defect Engineering in Cubic Cerium Oxide Nanostructures for Catalytic Oxidation, *Nano Lett.*, 2011, **11**(7), 2666–2671.
20 T. Mori, D. R. Ou, J. Zou and J. Drennan, Present status and future prospect of design of Pt–cerium oxide electrodes for fuel cell applications, *Prog. Nat. Sci.*, 2012, **22**(6), 561–571.
21 C. D'Urso, C. Oldani, V. Baglio, L. Merlo and A. S. Aricò, Towards fuel cell membranes with improved lifetime: Aquivion® Perfluorosulfonic Acid membranes containing immobilized radical scavengers, *J. Power Sources*, 2014, **272**, 753–758.
22 C. D'Urso, C. Oldani, V. Baglio, L. Merlo and A. S. Aricò, Immobilized transition metal-based radical scavengers and their effect on durability of Aquivion® perfluorosulfonic acid membranes, *J. Power Sources*, 2016, **301**, 317–325.
23 B. R. Bitner, D. C. Marcano, J. M. Berlin, R. H. Fabian, L. Cherian, J. C. Culver, M. E. Dickinson, C. S. Robertson, R. G. Pautler and T. A. Kent, Antioxidant carbon particles improve cerebrovascular dysfunction following traumatic brain injury, *ACS Nano*, 2012, **6**(9), 8007–8014.
24 A. Galano, Carbon nanotubes as free-radical scavengers, *J. Phys. Chem. C*, 2008, **112**(24), 8922–8927.
25 A. Martinez and A. Galano, Free radical scavenging activity of ultrashort single-walled carbon nanotubes with different structures through electron transfer reactions, *J. Phys. Chem. C*, 2010, **114**(18), 8184–8191.
26 J. Wei, J. Ding, X. Zhang, D. Wu, Z. Wang, J. Luo and K. Wang, Coated double-walled carbon nanotubes with ceria nanoparticles, *Mater. Lett.*, 2005, **59**(2), 322–325.
27 D.-J. Guo and Z.-H. Jing, A novel co-precipitation method for preparation of Pt–CeO_2 composites on multi-walled carbon nanotubes for direct methanol fuel cells, *J. Power Sources*, 2010, **195**(12), 3802–3805.
28 J. Wang, G. Yin, Y. Shao, Z. Wang and Y. Gao, Platinum deposition on multiwalled carbon nanotubes by ion-exchange method as electrocatalysts for oxygen reduction, *J. Electrochem. Soc.*, 2007, **154**(7), B687.
29 K. Maiti, N. H. Kim and J. H. Lee, Strongly stabilized integrated bimetallic oxide of Fe_2O_3–MoO_3 Nano-crystal entrapped N-doped graphene as a superior oxygen reduction reaction electrocatalyst, *Chem. Eng. J.*, 2021, **410**, 128358.
30 L. Wei, H. E. Karahan, S. Zhai, H. Liu, X. Chen, Z. Zhou, Y. Lei, Z. Liu and Y. Chen, Amorphous bimetallic oxide–graphene hybrids as bifunctional oxygen electrocatalysts for rechargeable Zn–air batteries, *Adv. Mater.*, 2017, **29**(38), 1701410.
31 C. Goswami, H. Saikia, K. Tada, S. Tanaka, P. Sudarsanam, S. K. Bhargava and P. Bharali, Bimetallic palladium–nickel nanoparticles anchored on carbon as high-performance electrocatalysts for oxygen reduction and formic acid oxidation reactions, *ACS Appl. Energy Mater.*, 2020, **3**(9), 9285–9295.
32 I. A. Khan, Y. Qian, A. Badshah, M. A. Nadeem and D. Zhao, Highly Porous Carbon Derived from MOF-5 as a Support of ORR Electrocatalysts for Fuel Cells, *ACS Appl. Mater. Interfaces*, 2016, **8**(27), 17268–17275.
33 H. Yang, K. Wang, Z. Tang, Z. Liu and S. Chen, Bimetallic PdZn nanoparticles for oxygen reduction reaction in alkaline medium: the effects of surface structure, *J. Catal.*, 2020, **382**, 181–191.
34 G. Bampos, S. Bebelis, D. I. Kondarides and X. Verykios, Comparison of the activity of Pd–M (M: Ag, Co, Cu, Fe, Ni, Zn) bimetallic electrocatalysts for oxygen reduction reaction, *Top. Catal.*, 2017, **60**(15), 1260–1273.
35 F. Nasim and M. A. Nadeem, Understanding the mechanism and synergistic interaction of cobalt-based electrocatalysts containing nitrogen-doped carbon for 4 e^- ORR, *J. Mater. Chem. A*, 2023, **11**(19), 10095–10124.
36 F. Nasim, H. Ali, M. A. Nadeem and M. A. Nadeem, High-performance FeO_x@CoO_x/NC electrocatalysts for the oxygen reduction reaction in alkaline media. *Sustain*, *Energy Fuels*, 2023, **7**(1), 190–200.
37 B. Liu, R. Wang, Y. Yao, J. Ma, Y. Sun, J. Wan, Y. Zhang, S. Wang and J. Zou, Hollow-structured CoP nanotubes wrapped by N-doped carbon layer with interfacial charges polarization for efficiently boosting oxygen reduction/evolution reactions, *J. Chem. Eng.*, 2022, **431**, 133238.
38 S. Li, R. Wang, X. Yang, J. Wu, H. Meng, H. Xu and Z. Ren, Binary metal phosphides with MoP and FeP embedded in P,N-doped graphitic carbon as electrocatalysts for oxygen reduction, *ACS Sustainable Chem. Eng.*, 2019, **7**(13), 11872–11884.
39 A. Parra-Puerto, K. L. Ng, K. Fahy, A. E. Goode, M. P. Ryan and A. Kucernak, Supported transition metal phosphides: activity survey for HER, ORR, OER, and corrosion resistance in acid and alkaline electrolytes, *ACS Catal.*, 2019, **9**(12), 11515–11529.
40 T. Zhou, N. Zhang, C. Wu and Y. Xie, Surface/interface nanoengineering for rechargeable Zn–air batteries, *Energy Environ. Sci.*, 2020, **13**(4), 1132–1153.
41 H. Cheng, K. Xu, L. Xing, S. Liu, Y. Gong, L. Gu, L. Zhang and C. Wu, Manganous oxide nanoparticles encapsulated in few-layer carbon as an efficient electrocatalyst for oxygen reduction in alkaline media, *J. Mater. Chem. A*, 2016, **4**(30), 11775–11781.
42 C. Yao, J. Li, Z. Zhang, C. Gou, Z. Zhang, G. Pan and J. Zhang, Hierarchical Core–Shell Co2N/CoP Embedded in

N,P-doped Carbon Nanotubes as Efficient Oxygen Reduction Reaction Catalysts for Zn-air Batteries, *Small*, 2022, **18**(20), 2108094.

43 S. H. Ahn and A. Manthiram, Cobalt Phosphide Coupled with Heteroatom-Doped Nanocarbon Hybrid Electroctalysts for Efficient, Long-Life Rechargeable Zinc–Air Batteries, *Small*, 2017, **13**(40), 1702068.

44 T. Li, Y. Wu and M. Pei, Screening of transition metal single-atom catalysts doped on γ-graphyne-like BN sheet for efficient nitrogen reduction reaction, *J. Alloys Compd.*, 2022, **908**, 164675.

45 H. Wei, X. Su, J. Liu, J. Tian, Z. Wang, K. Sun, Z. Rui, W. Yang, Z. Zou and A. CeO2, modified phenylenediamine-based Fe/N/C with enhanced durability/stability as non-precious metal catalyst for oxygen reduction reaction, *Electrochem. Commun.*, 2018, **88**, 19–23.

46 Y. Zheng, A. S. Petersen, H. Wan, R. Hübner, J. Zhang, J. Wang, H. Qi, Y. Ye, C. Liang and J. Yang, Scalable and Controllable Synthesis of Pt–Ni Bunched-Nanocages Aerogels as Efficient Electrocatalysts for Oxygen Reduction Reaction, *Adv. Energy Mater.*, 2023, **13**(20), 2204257.

47 T. M. Pham, K. Im and J. Kim, A highly stable tungsten-doped TiO_2-supported platinum electrocatalyst for oxygen reduction reaction in acidic media, *Appl. Surf. Sci.*, 2023, **611**, 155740.

48 J.-H. Park, K. Kim, X. Wang, M. Huda, Y. Sawada, Y. Matsuo, N. Saito and M. Kawasumi, Highly durable graphene-encapsulated platinum-based electrocatalyst for oxygen reduction reactions synthesized by solution plasma process, *J. Power Sources*, 2023, **580**, 233419.

49 W. Shi, H.-U. Park, A.-H. Park, L. Xue, S.-K. Kim, G.-G. Park and Y.-U. Kwon, Boosting electrocatalytic performance and durability of Pt nanoparticles by conductive MO_{2-x} (M = Ti, Zr) supports, *Appl. Catal., B*, 2023, **331**, 122692.

50 Y. Liu, M. Wu, S. Sheng, C. Zhi, Y. Wang and X. Li, The fabrication of Pt–Pb alloy networks with high-density micropores by dealloying for enhanced oxygen reduction activity, *Int. J. Hydrogen Energy*, 2023, **48**(36), 13470–13478.

51 S. Wang, T. Sheng and Q. Yuan, Low-Pt Octahedral PtCuCo Nanoalloys:''One Stone, Four Birds'' for Oxygen Reduction and Methanol Oxidation Reactions, *Inorg. Chem.*, 2023, **62**(29), 11581–11588.

52 F. Qian, C. Hu, W. Jiang, J. Zhang, L. Peng, L. Song and Q. Chen, General and scalable strategy for synthesis of Pt-rare earth alloys as highly durable oxygen reduction electrocatalysts, *J. Chem. Eng.*, 2023, **468**, 143665.

53 Y. Jiang, Y. Wang, J. Qian, Y. Mu, Z. Li, T. Zhao and L. Zeng, Durable carbon-shell-encapsulated Pt/C catalysts synthesized by direct pyrolysis of Pt-pyrrole complexes for the oxygen reduction reaction, *Int. J. Hydrogen Energy*, 2023, **51**, 578–586.